Supporting Information

Problems With Solutions: Manipulating Alkylammonium Additive Reactivity for Durable High-Quality Perovskite Films

Jack R. Palmer[1], Soichiro Iwamoto[2], Clark Han[2], Connor J. Dolan[2], Hendrik M. Vossler[1], Sean P. Dunfield[2], David P. Fenning[1,2*]*

[1]Materials Science and Engineering Program, University of California, San Diego, La Jolla, California 92093, USA

[2]Department of Chemical and Nano Engineering, University of California, San Diego, La Jolla, California 92093, USA

*Correspondence to: dfenning@eng.ucsd.edu, seandunfield@gmail.com

Supplementary Note on NMR

Quantification of RACl reaction products and reaction rates

Using the reaction scheme presented in Figure 1a of the main text, structures for the reaction products of the alkylammonium with FA were determined. In the series of NMR spectra taken over 5 days, a unique resonance from the protons of the methylene group adjacent to the nitrogen atom was identified for each additive (except NH_4, for which no reaction product was observed). A convex hull baseline was subtracted from each peak and the area under the peak was calculated using trapezoidal integration. Next, this integrated intensity was normalized by the number of protons in that chemical environment, then divided by the FA C-H proton peak area, which was taken to be a constant concentration of 0.5M, thus converting the reaction product peak intensity to molarity. This procedure was carried out across all 5 days of spectra for each additive, and reaction product concentrations were plotted against time, to which lines were fitted to determine the reaction rates of each additive.

Figure S1. Molecular structures of alkylammoniums used in this study together with their names and abbreviations.

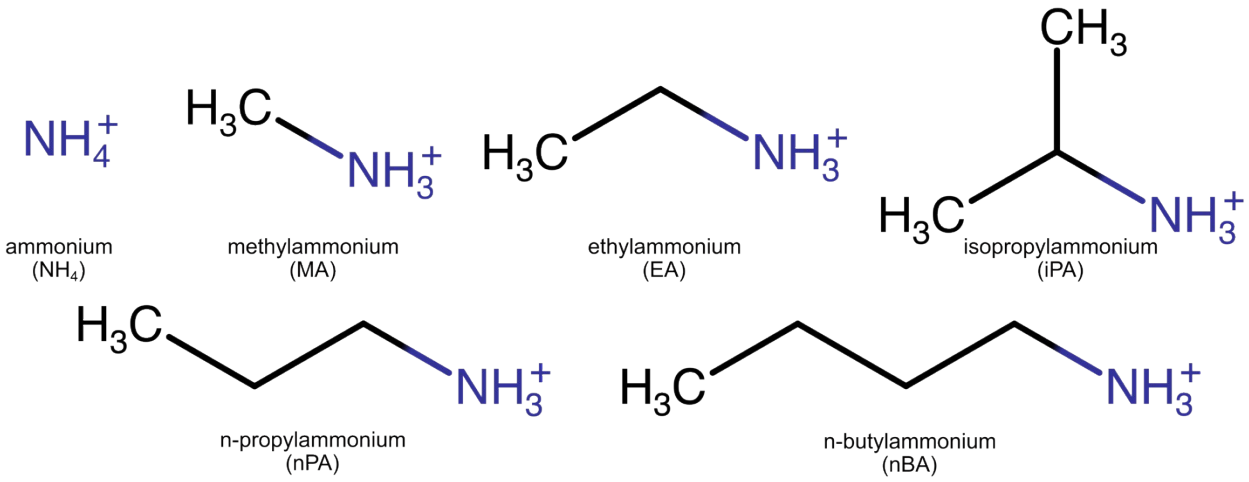

Figure S2. X-ray diffractograms of films produced from Fresh inks with (a) NH_4Cl, (b) MACl, and (c) EACl additives.

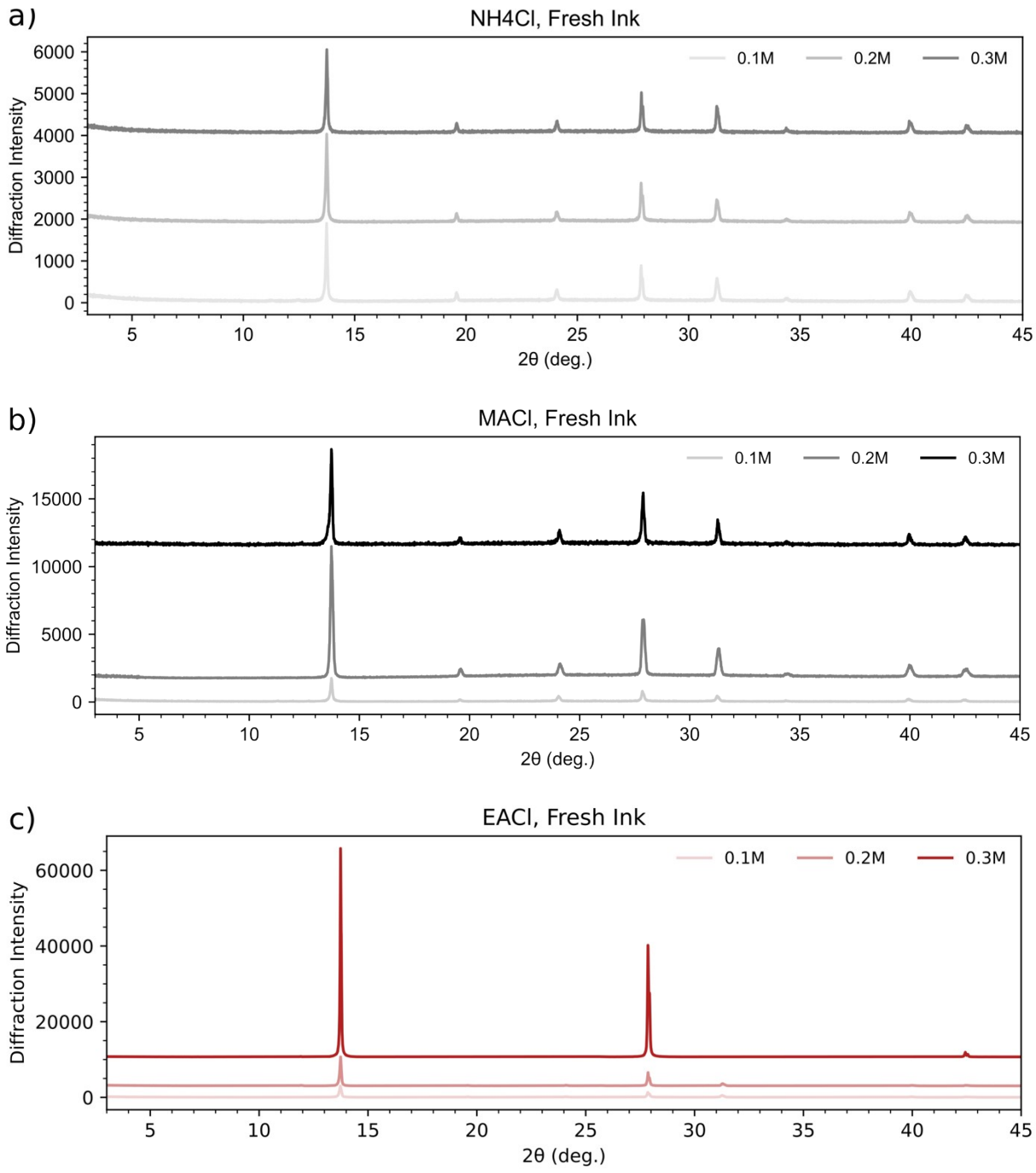

Figure S3. X-ray diffractograms of films produced from Fresh inks with (a) iPACl, (b) nPACl, and (c) nBACl additives.

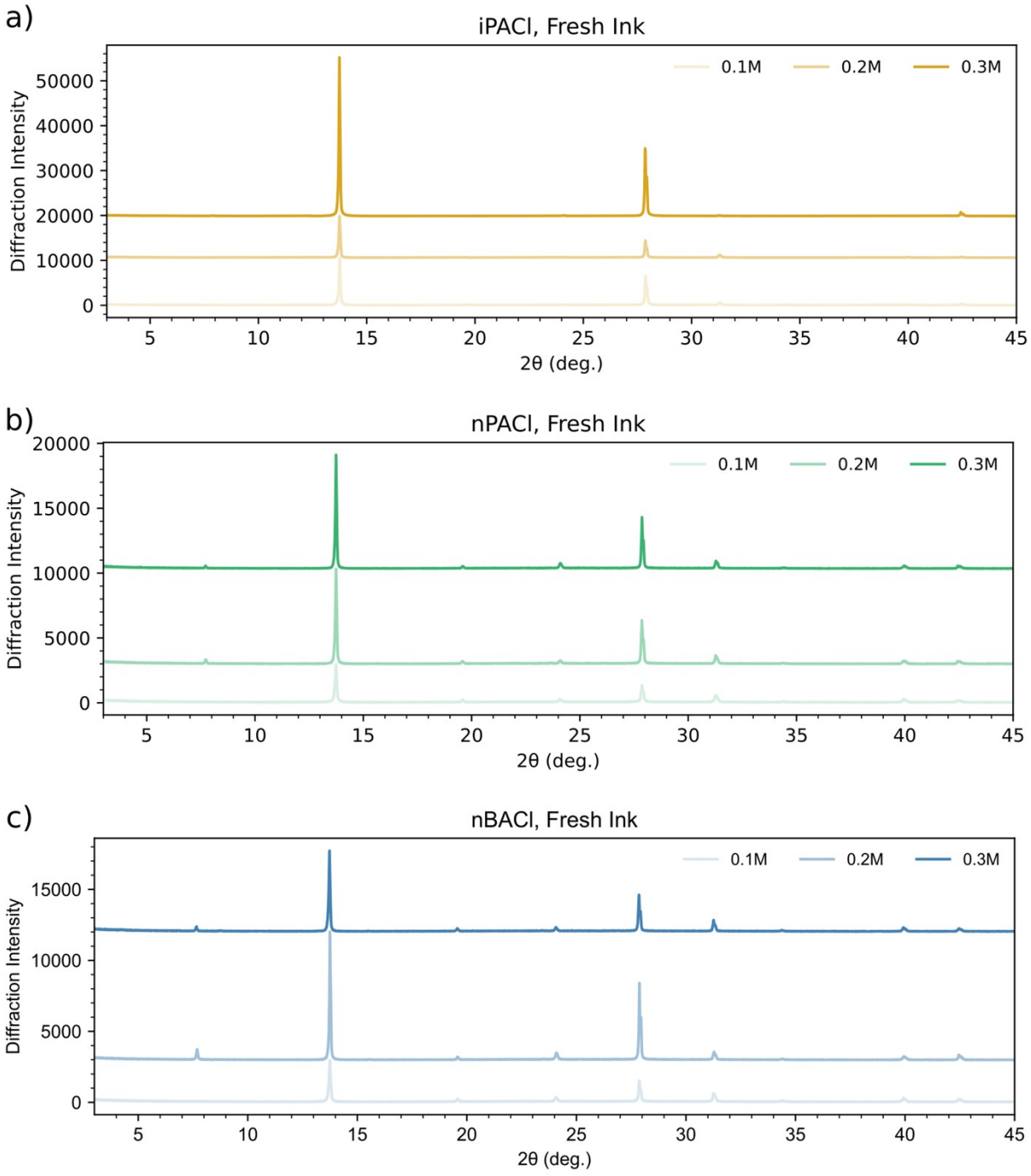

Figure S4. X-ray diffractograms of films produced from Aged inks with (a) NH_4Cl, (b) MACl, and (c) EACl additives.

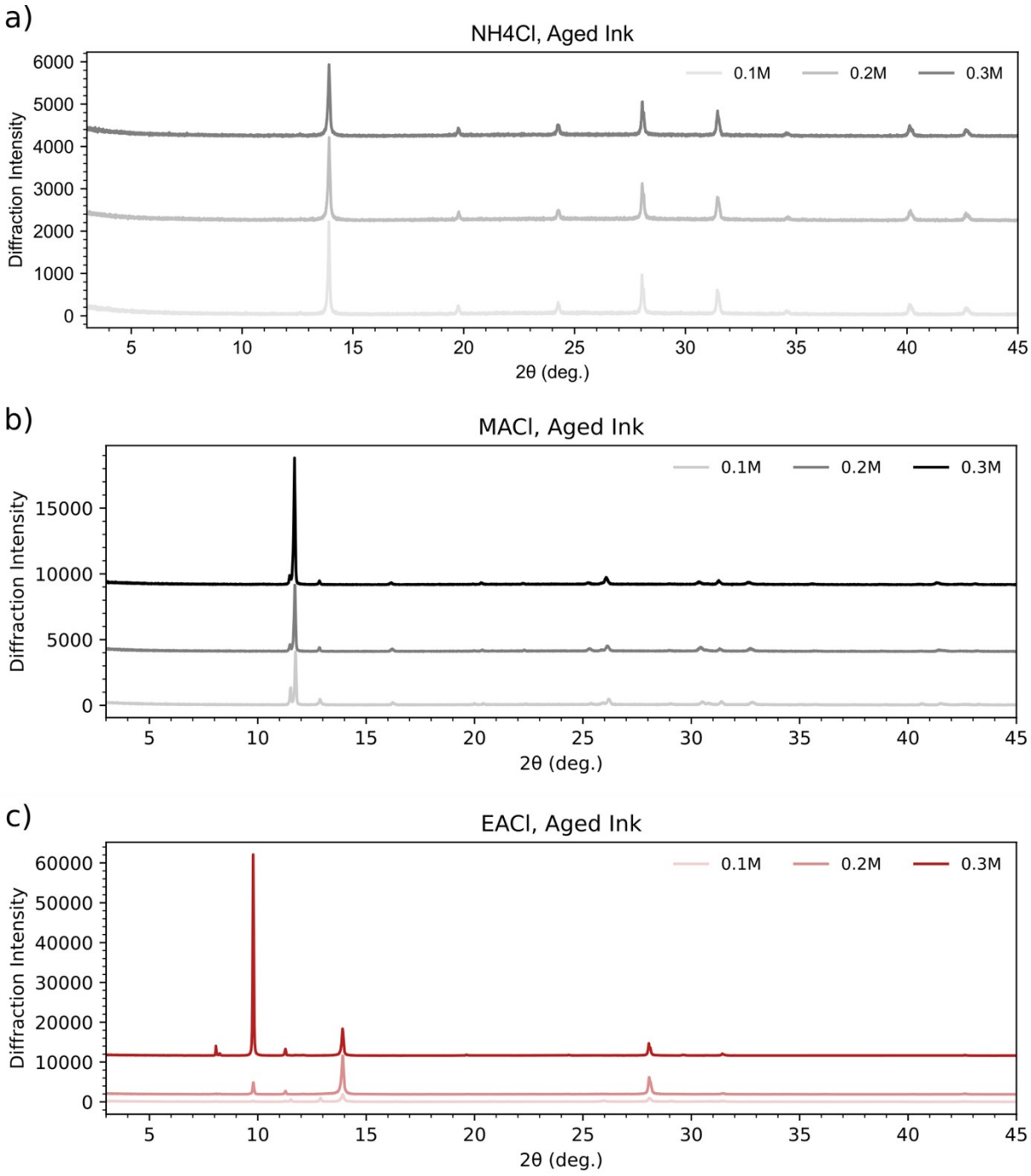

Figure S5. X-ray diffractograms of films produced from Aged inks for (a) iPACl, (b) nPACl, and (c) nBACl additives.

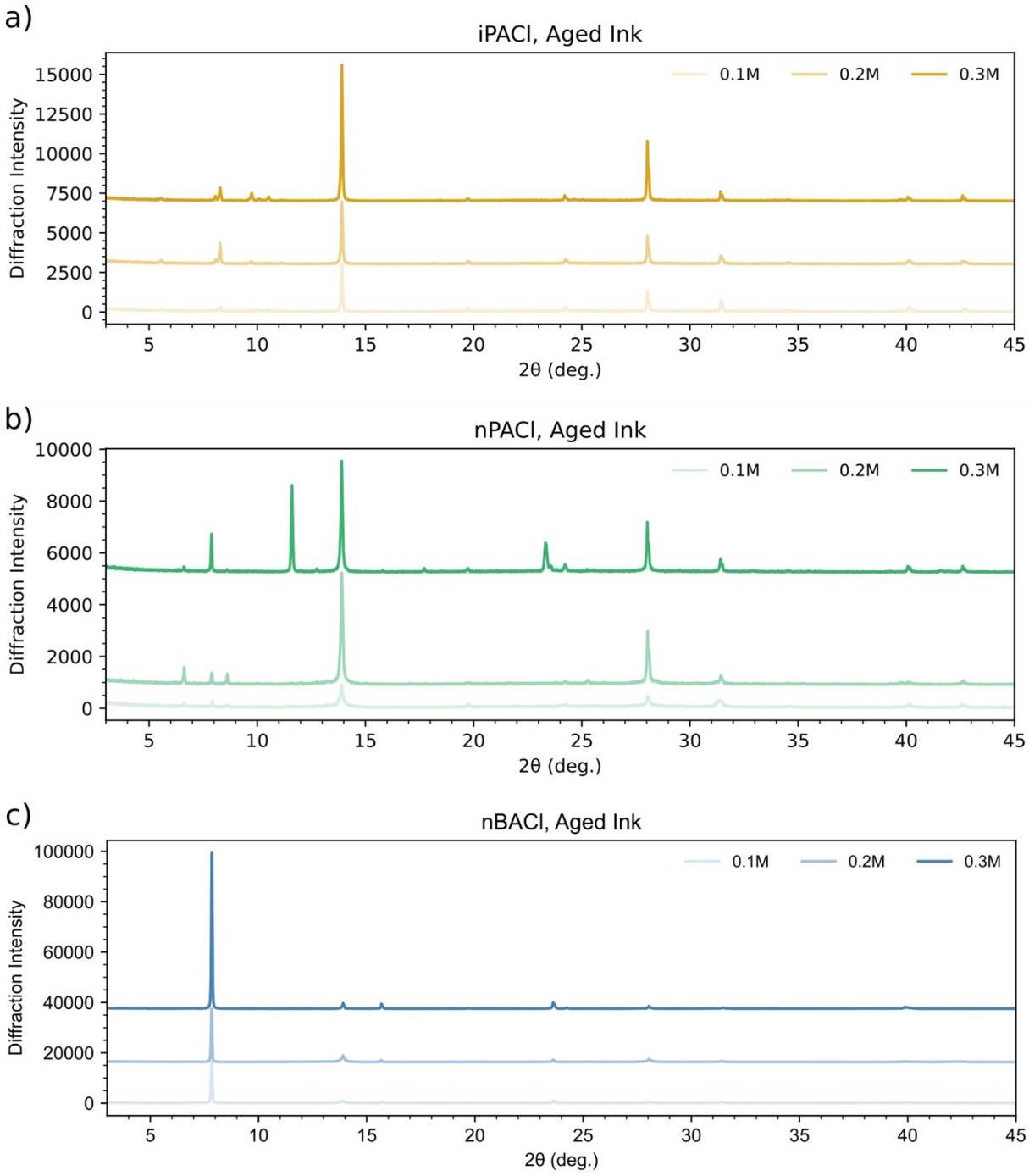

Figure S6. X-ray diffractograms of films produced from Fresh inks with (a) NH_4Cl, (b) MACl, and (c) EACl additives. Patterns are displayed on a semi-log plot to accentuate minor phases.

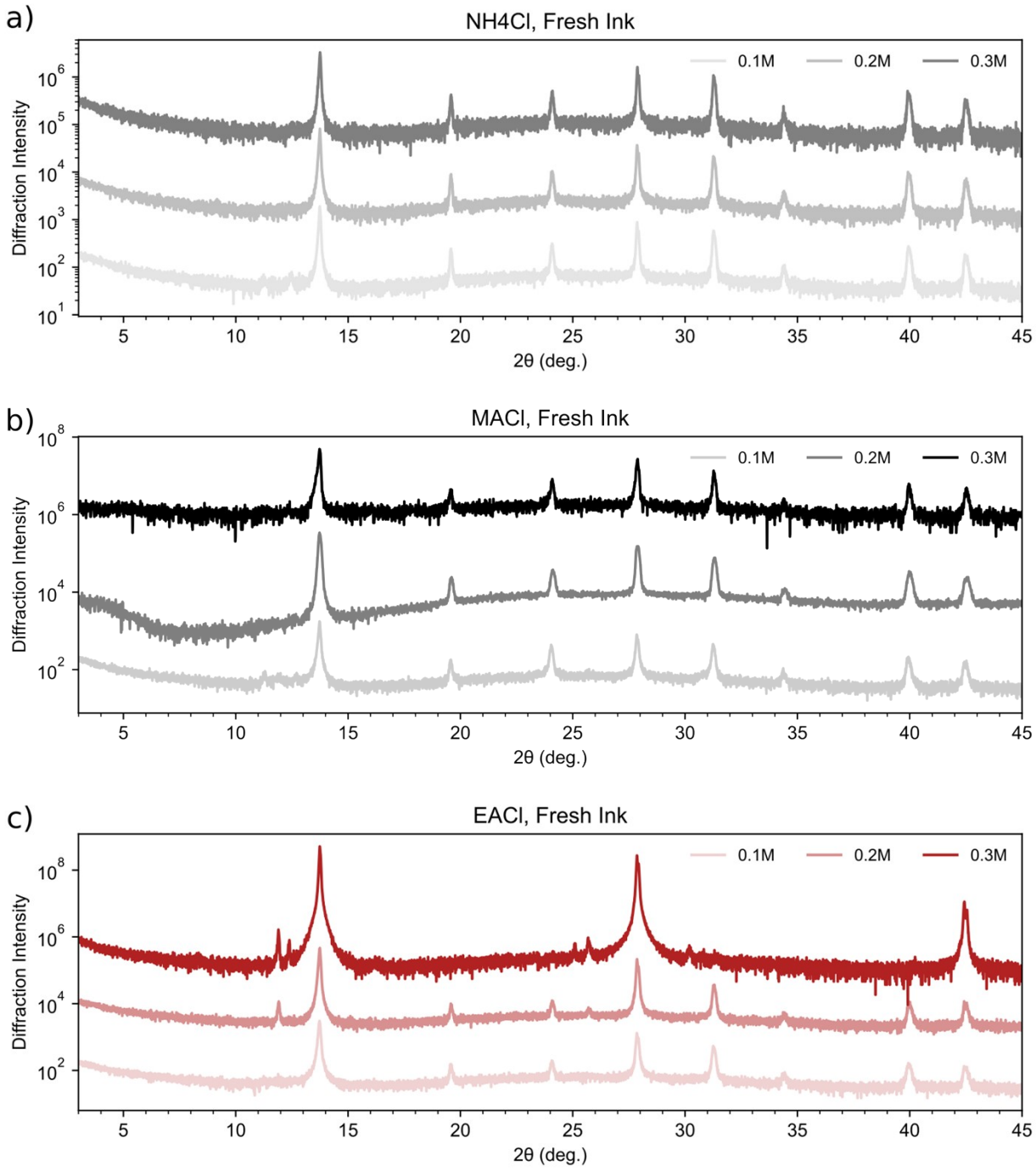

Figure S7. X-ray diffractograms of films produced from Fresh inks with (a) iPACl, (b) nPACl, and (c) nBACl additives. Patterns are displayed on a semi-log plot to accentuate minor phases.

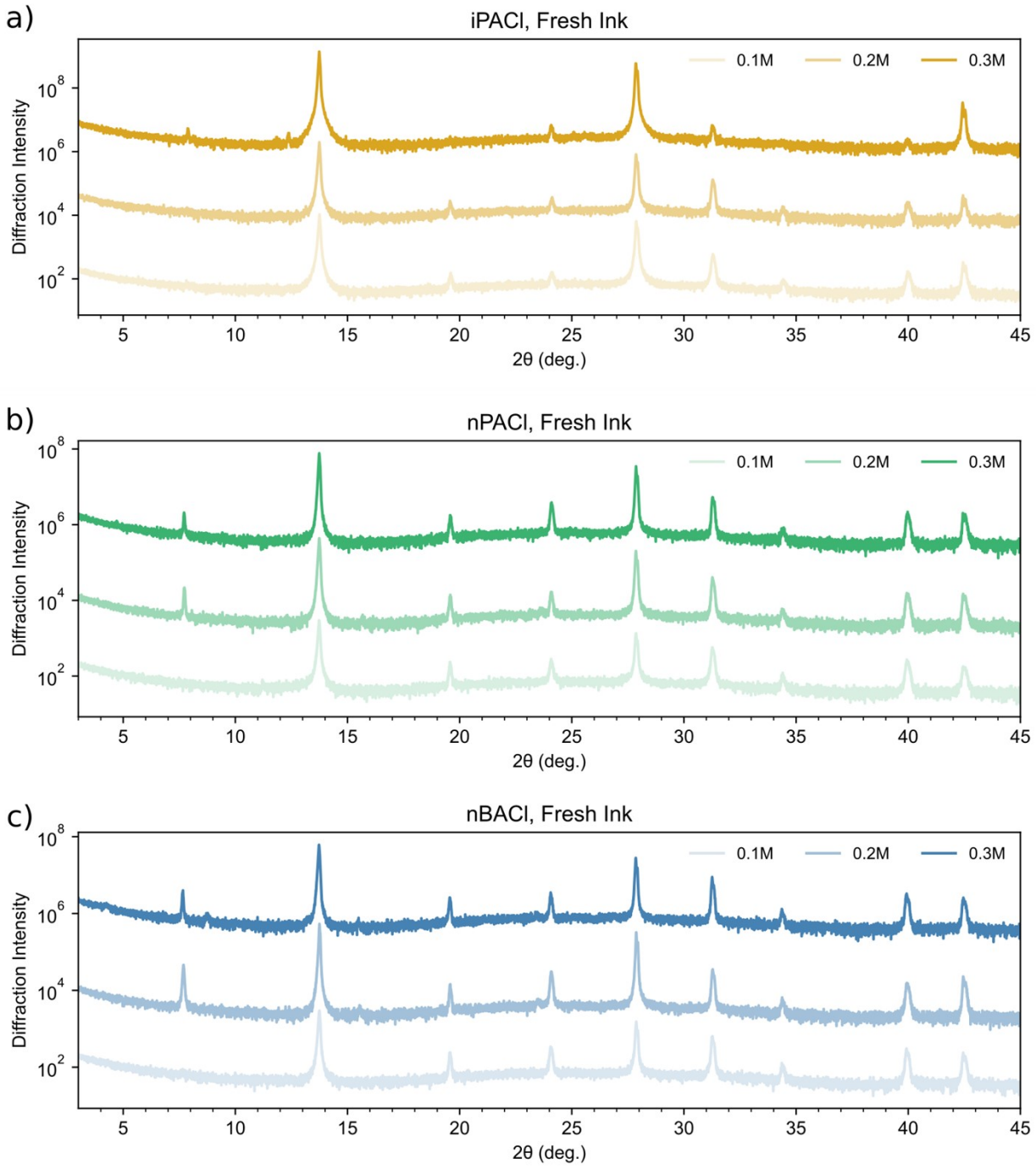

Figure S8. X-ray diffractograms of films produced from Aged inks with (a) NH_4Cl, (b) MACl, and (c) EACl additives. Patterns are displayed on a semi-log plot to accentuate minor phases

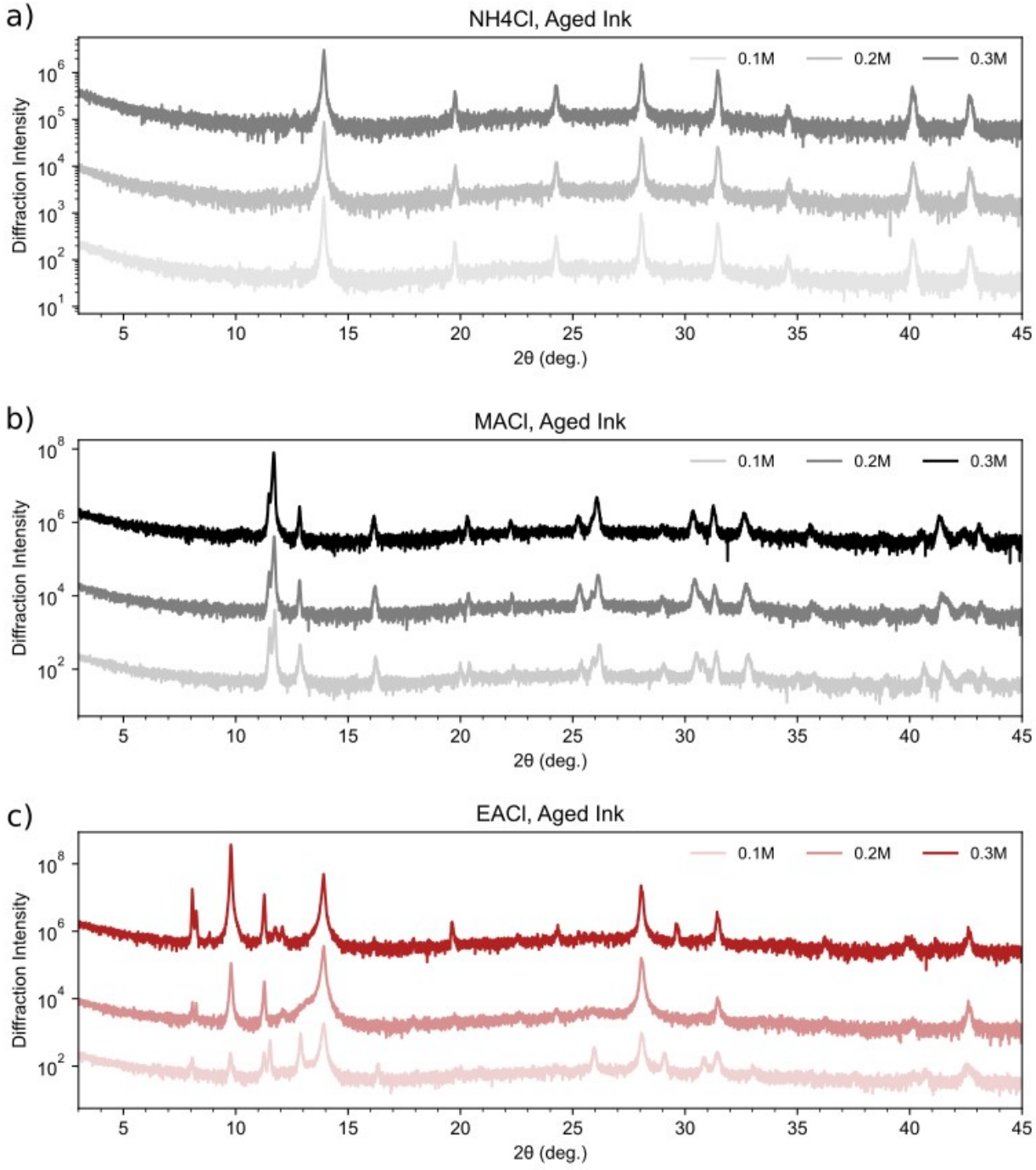

Figure S9. X-ray diffractograms of films produced from Aged inks with (a) iPACl, (b) nPACl, and (c) nBACl additives. Patterns are displayed on a semi-log plot to accentuate minor phases.

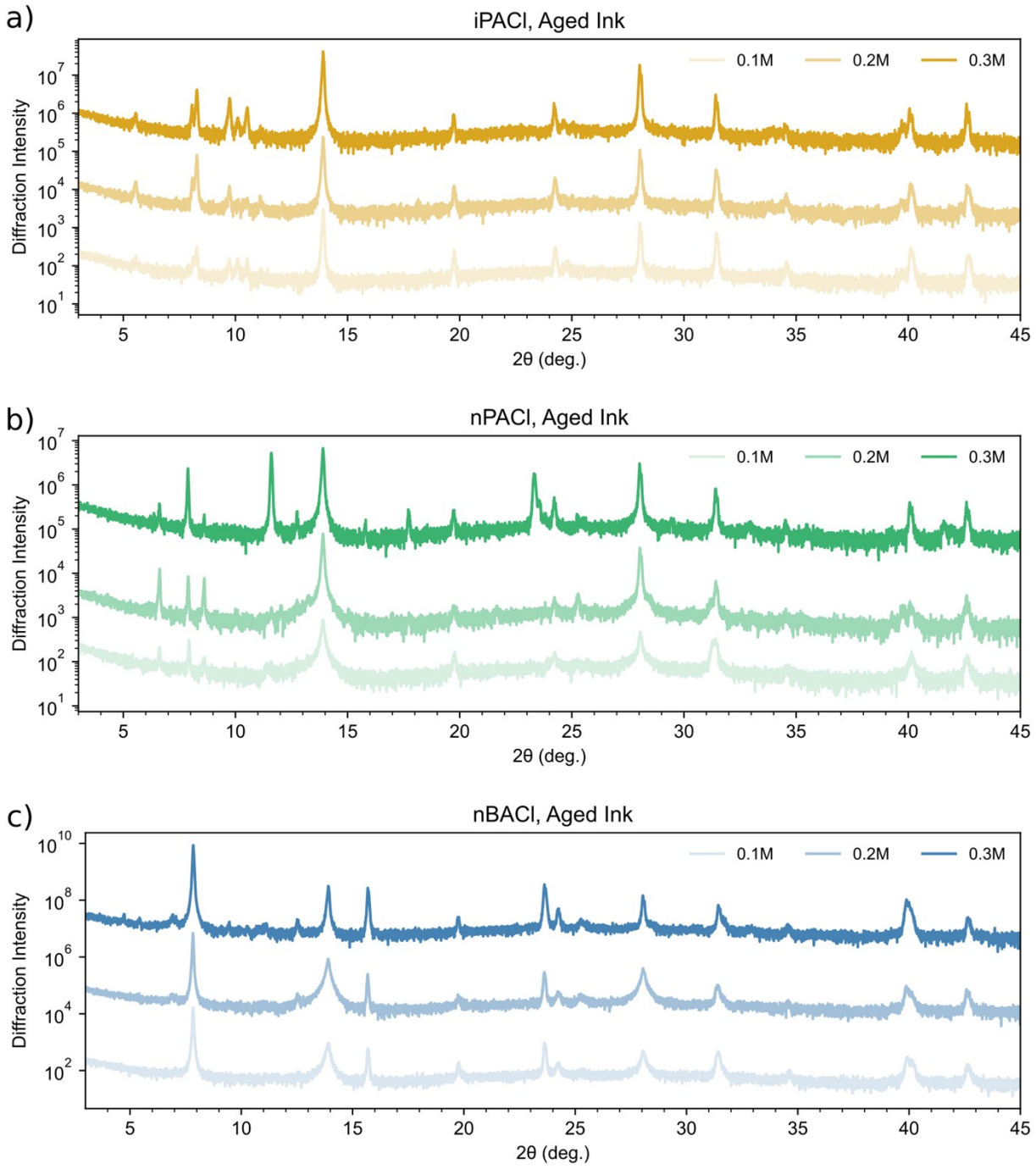

Figure S10. ATR-FTIR zoomed on the alkyl stretching region. ATR-FTIR transmittance data were transformed using -$\log_{10}$(%T/100) after a convex hull baseline subtraction. Dashed vertical lines indicate stretching vibrational modes unique to the additive's reaction product with FA.

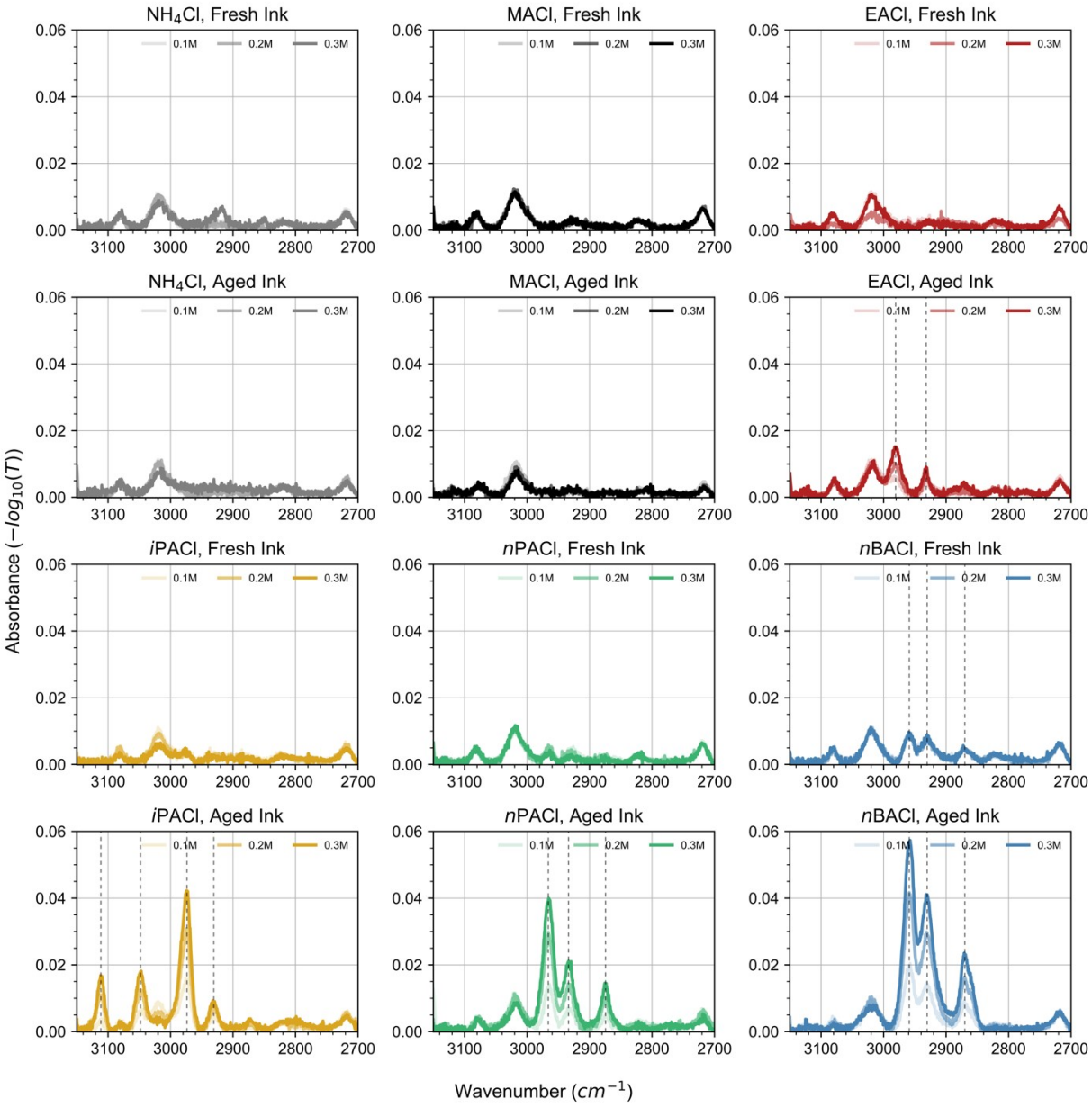

Figure S11. ATR-FTIR of films zoomed on the alkyl bending region. ATR-FTIR transmittance data were transformed using -$\log_{10}$(%T/100) after a convex hull baseline subtraction. Dashed vertical lines indicate bending vibrational modes unique to the additive's reaction product with FA.

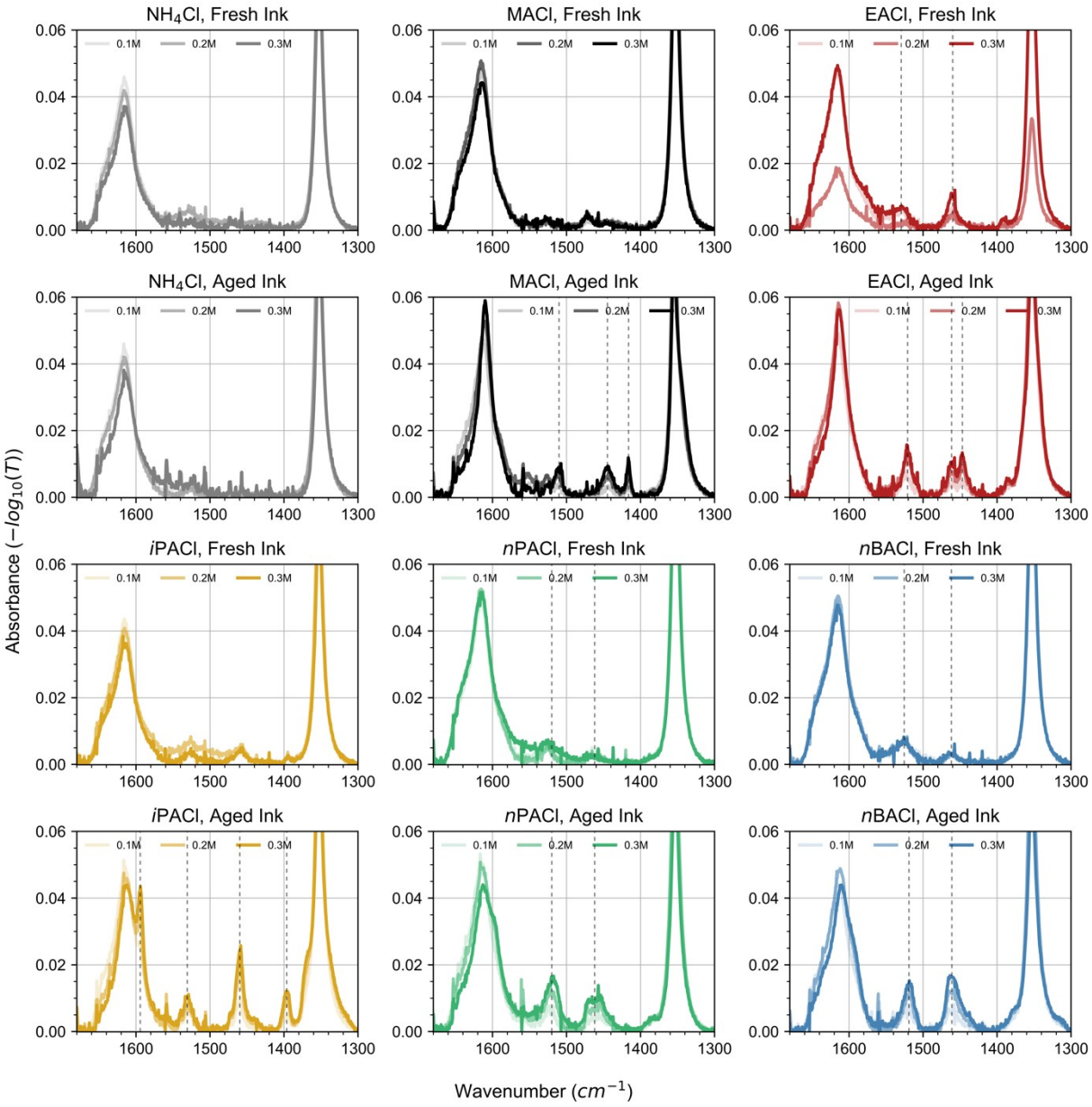

Figure S12. Full width at half maximum (FWHM) of the (001) perovskite diffraction peak.

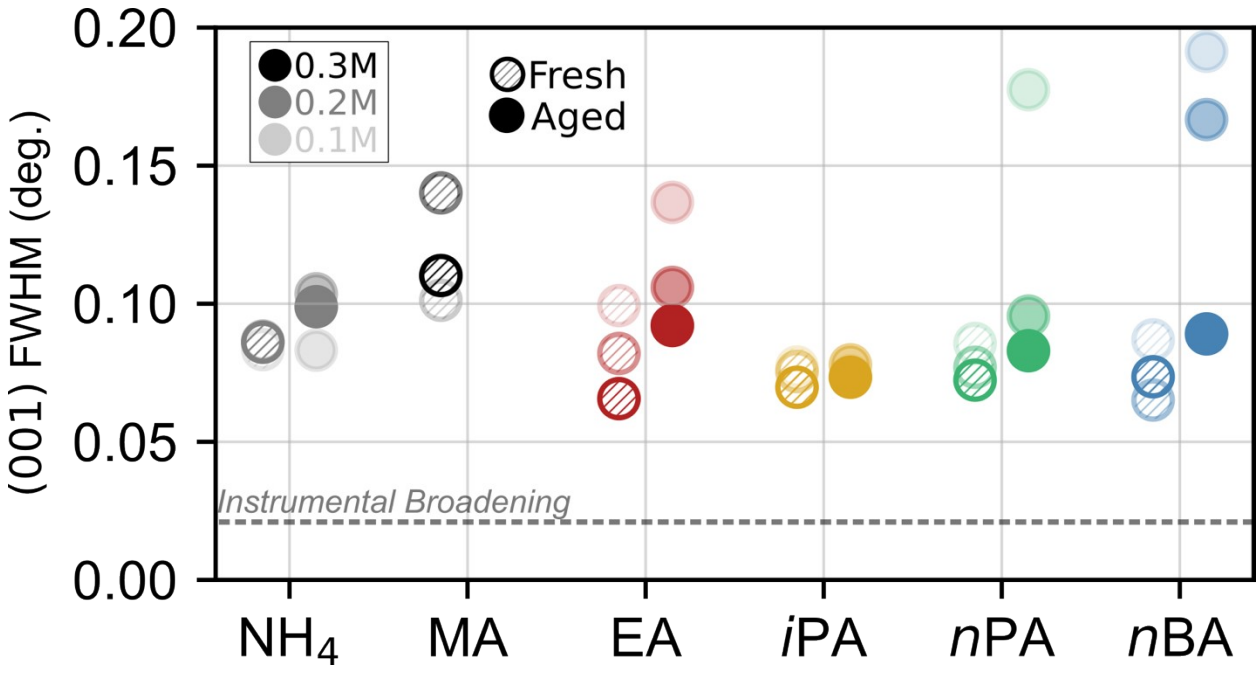

Figure S13. Microstrain extracted from Williamson-Hall analysis done on full diffraction patterns. Error bars shown are one standard deviation.

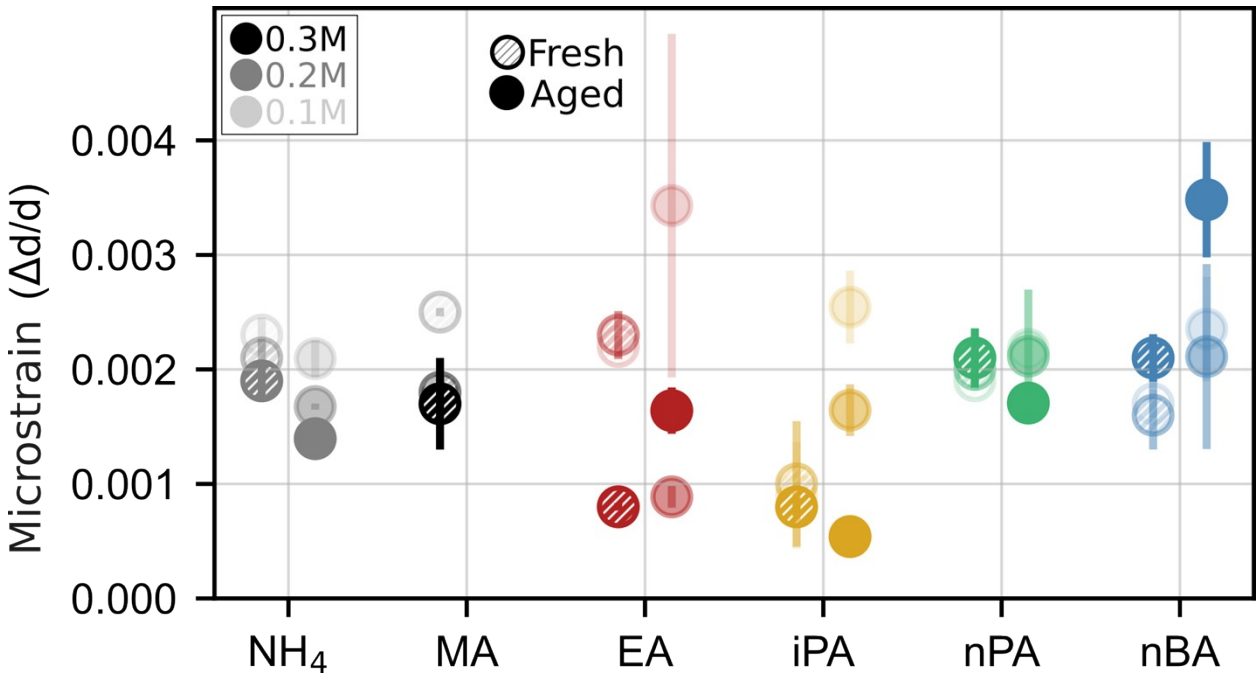

Figure S14. Williamson-Hall plots of XRD data across all sample conditions. Markers and line saturation increases in order of increasing additive concentration (0.1M, 0.2M, 0.3M).

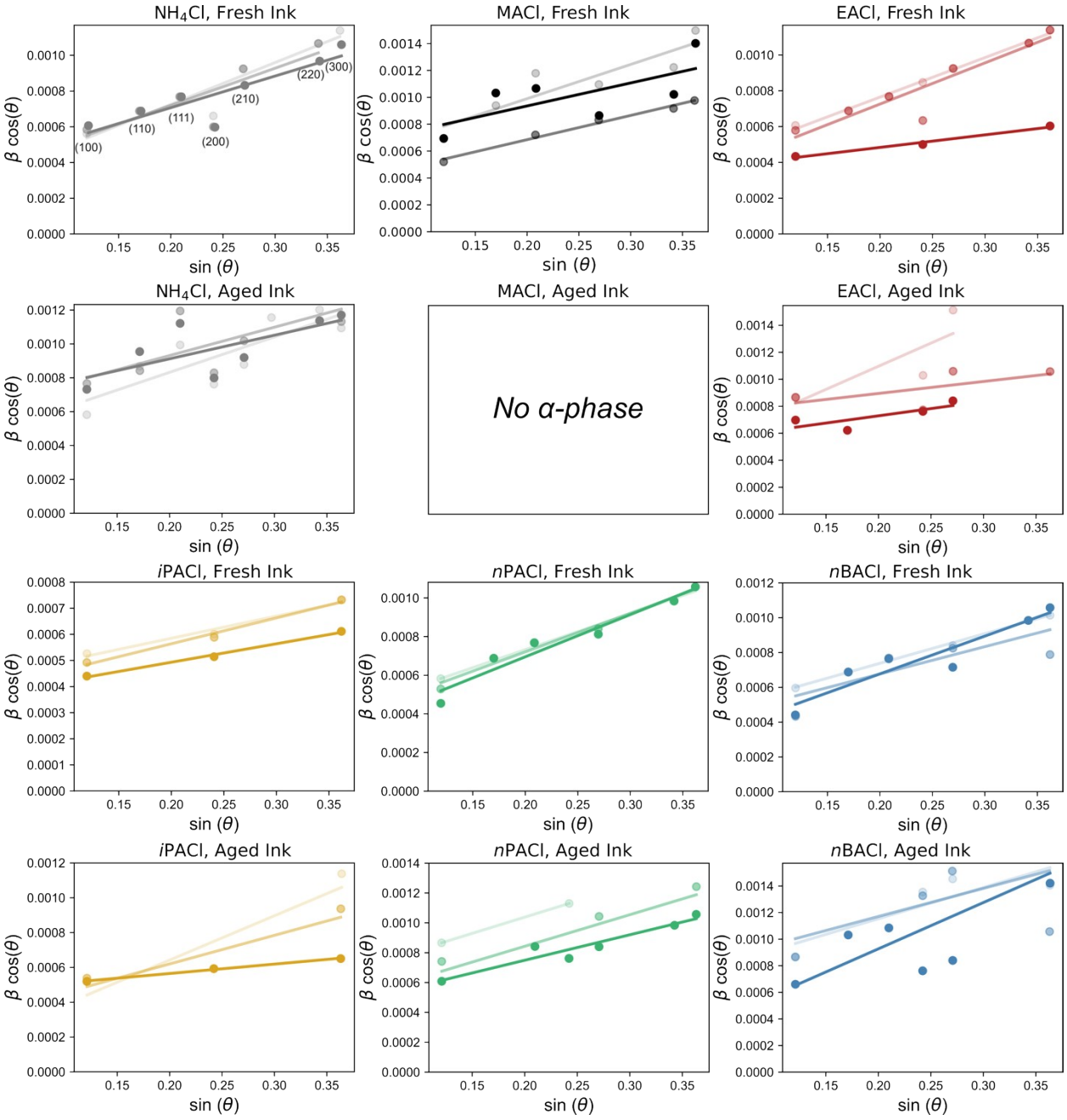

Figure S15. Total integrated diffraction intensity from 5˚-12˚ 2θ, displayed on a semi-log plot.

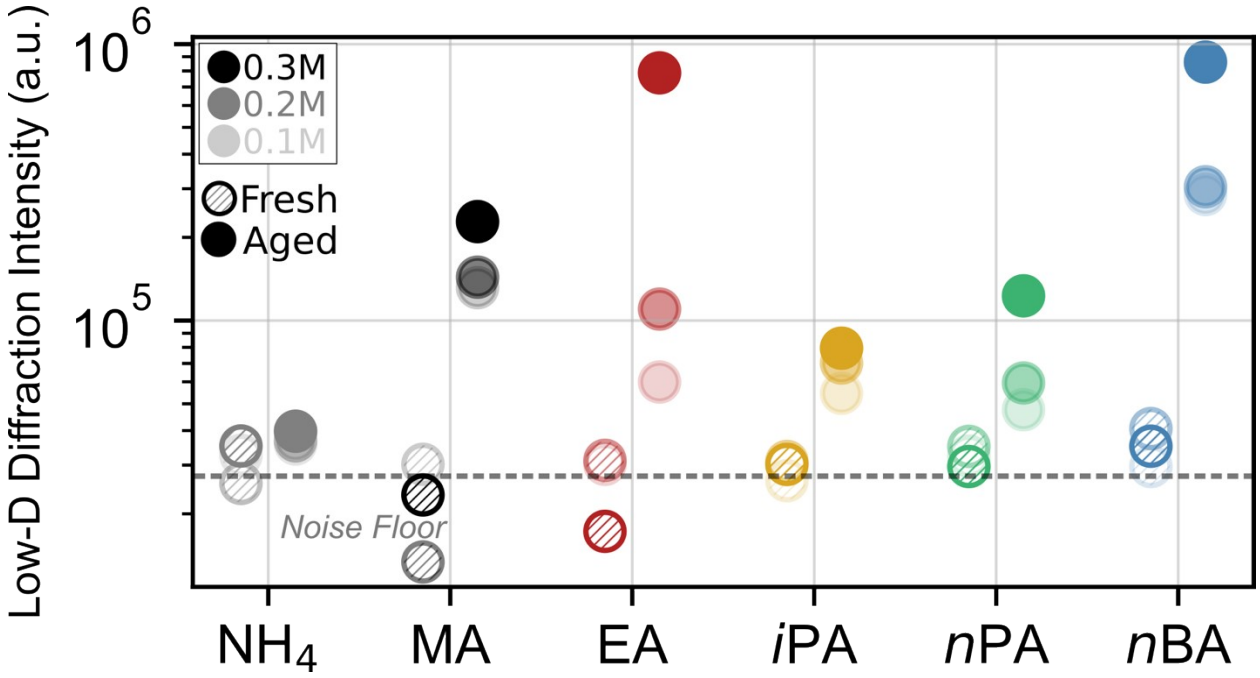

Figure S16. Camera images of 1"x1" films prepared with 0.1M RACl additive.

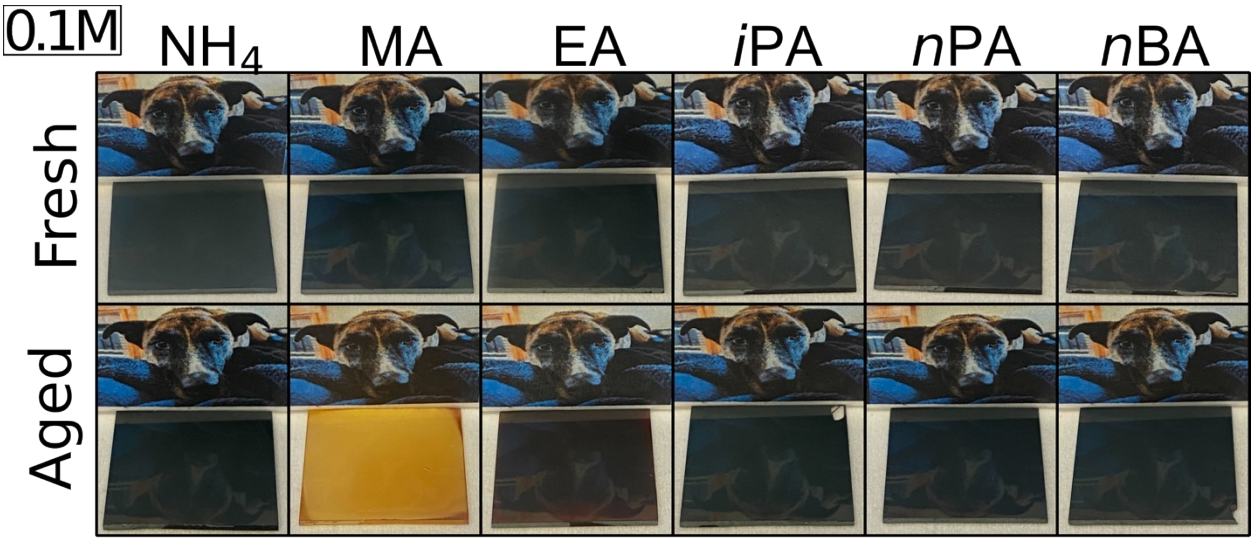

Figure S17. Camera images of 1"x1" films prepared with 0.2M RACl additive.

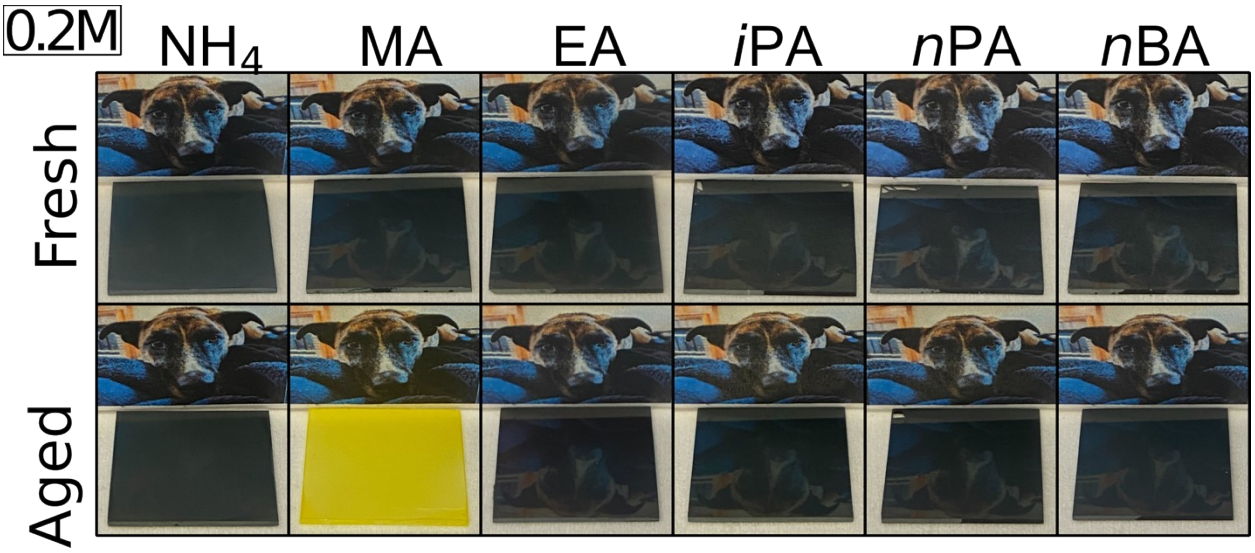

Figure S18. Camera images of 1"x1" films prepared with 0.3M RACl additive.

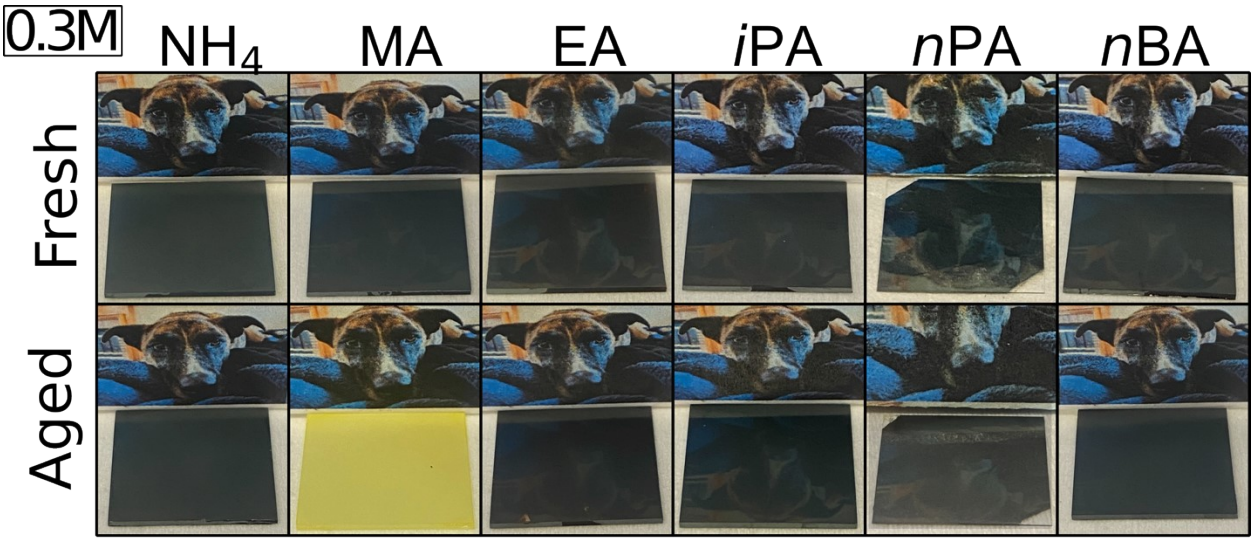

Figure S19. SEM micrographs of films prepared with 0.1M RACl additive.

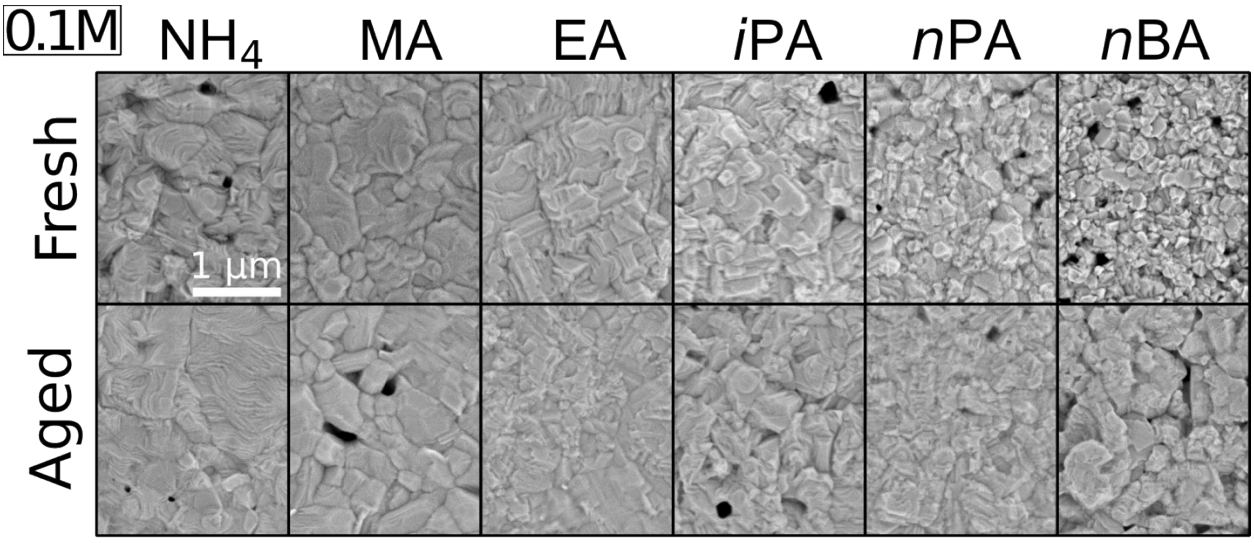

Figure S20. SEM micrographs of films prepared with 0.3M RACl additive.

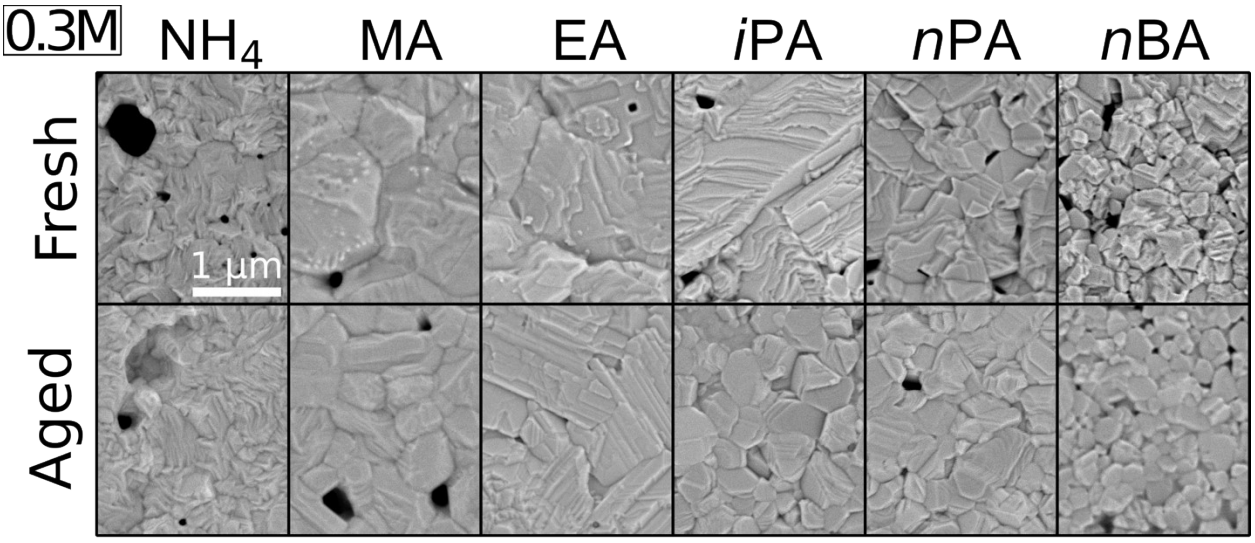

Figure S21. Photoluminescence spectra of all conditions, displayed on a linear scale

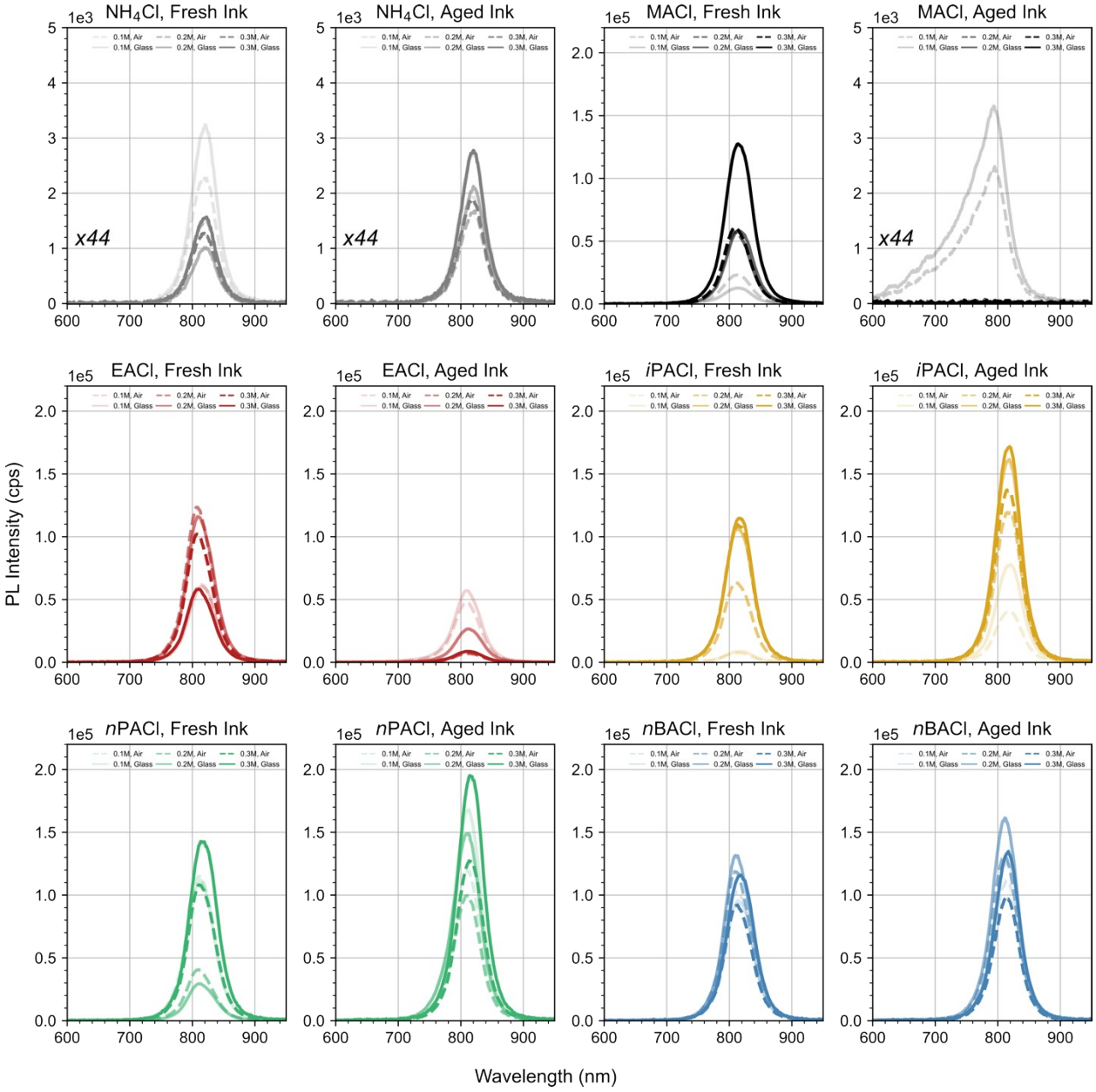

Figure S22. Photoluminescence spectra of all conditions, displayed on a semi-log scale

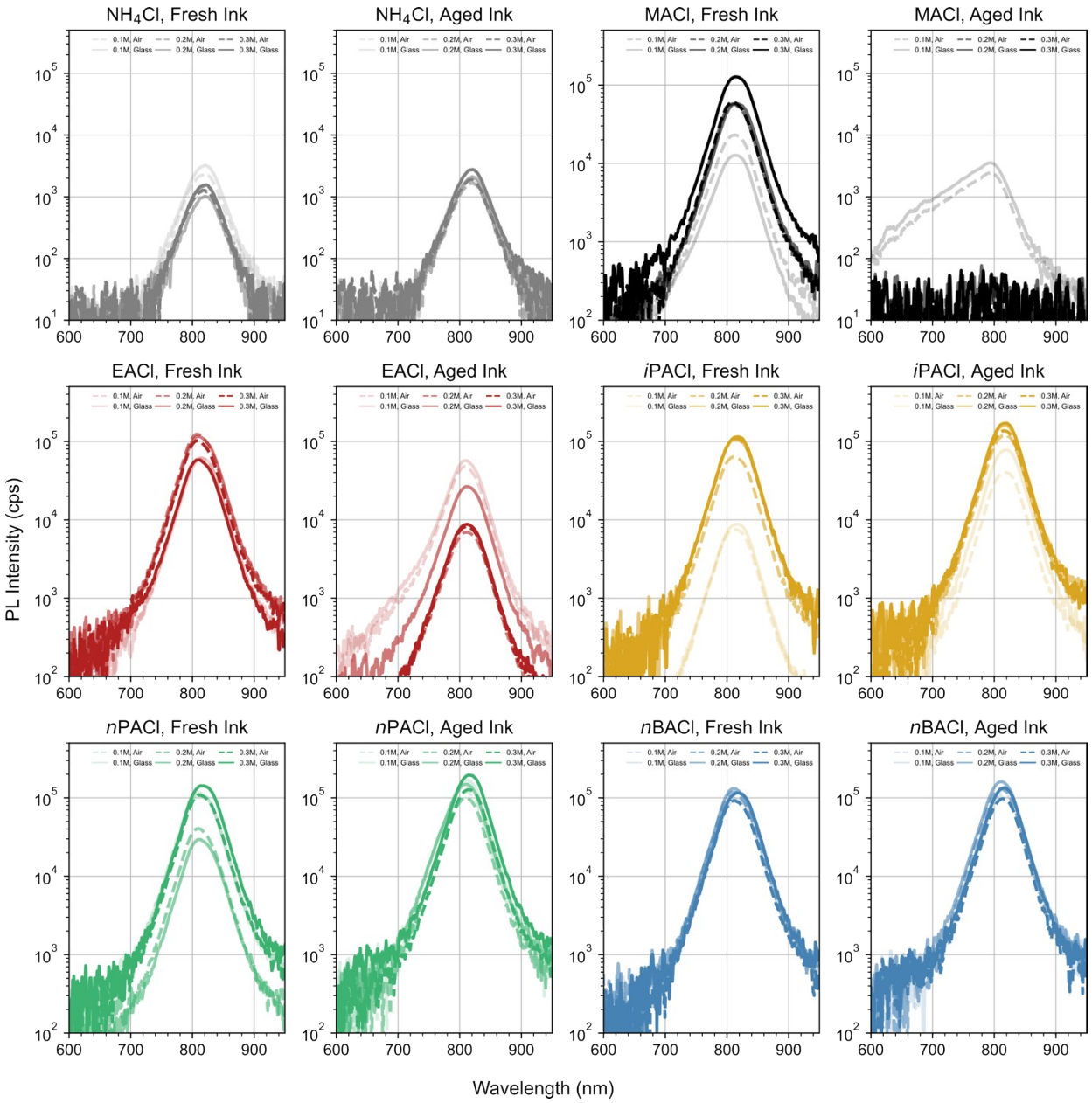

Figure S23. Implied JV curves of (a) Fresh and (b) Aged films from intensity-dependent PLQY measurements. (c) Implied power conversion efficiencies calculated from (a) and (b)

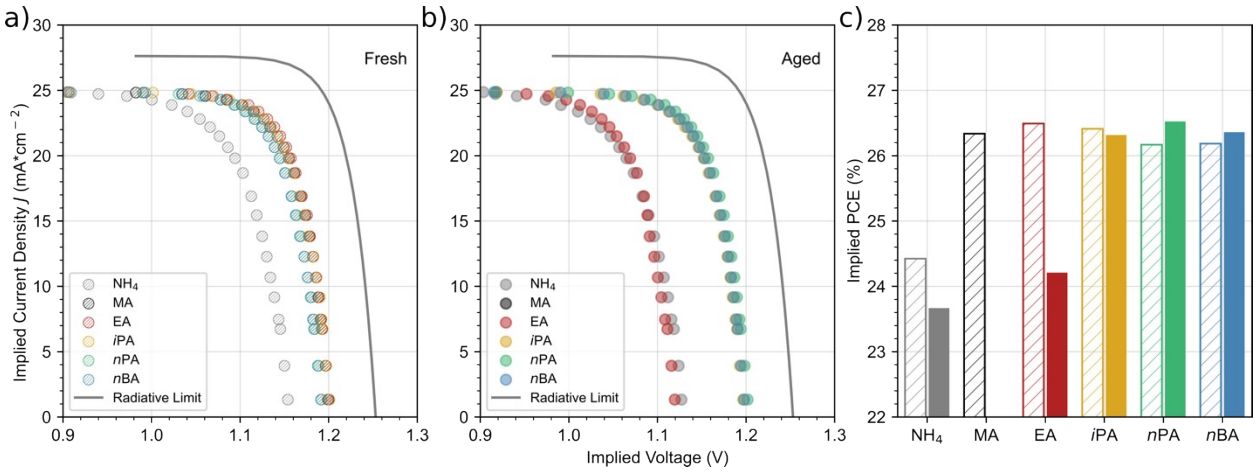

Figure S24. Red pixel intensity over time for degradation experiments. The solid line represents the average over film area while the shaded region is the sample standard deviation across that area.

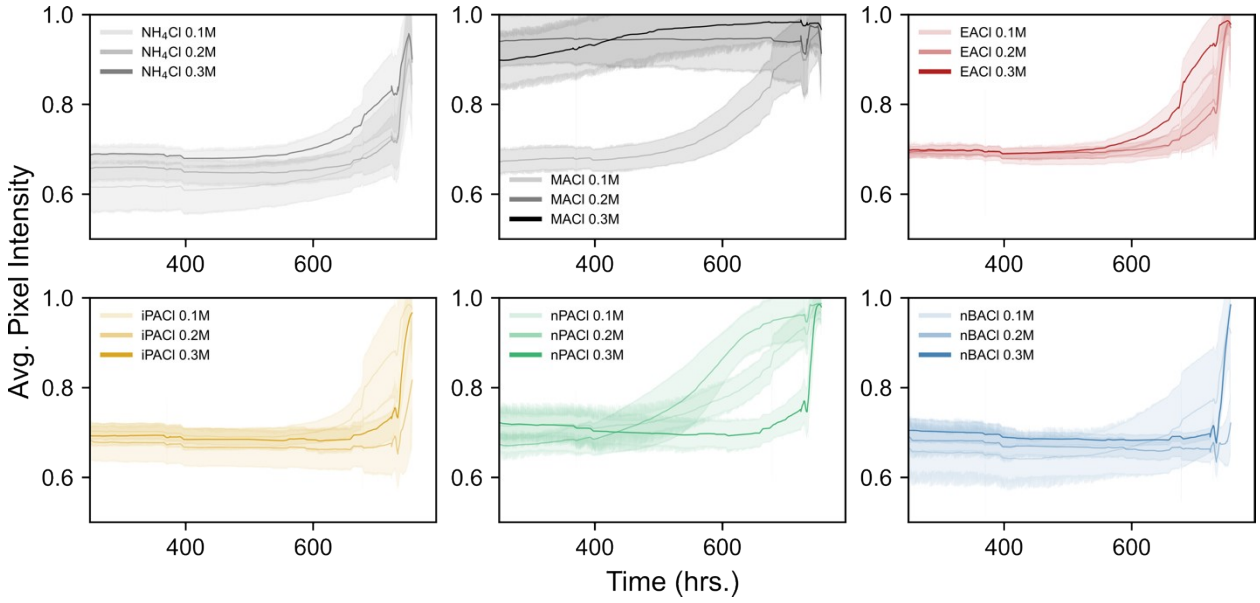

Figure S25: Spectral irradiance of the Viparspectra XS4000 used as the solar simulator light source during ISOS-L-2 degradation testing of films.

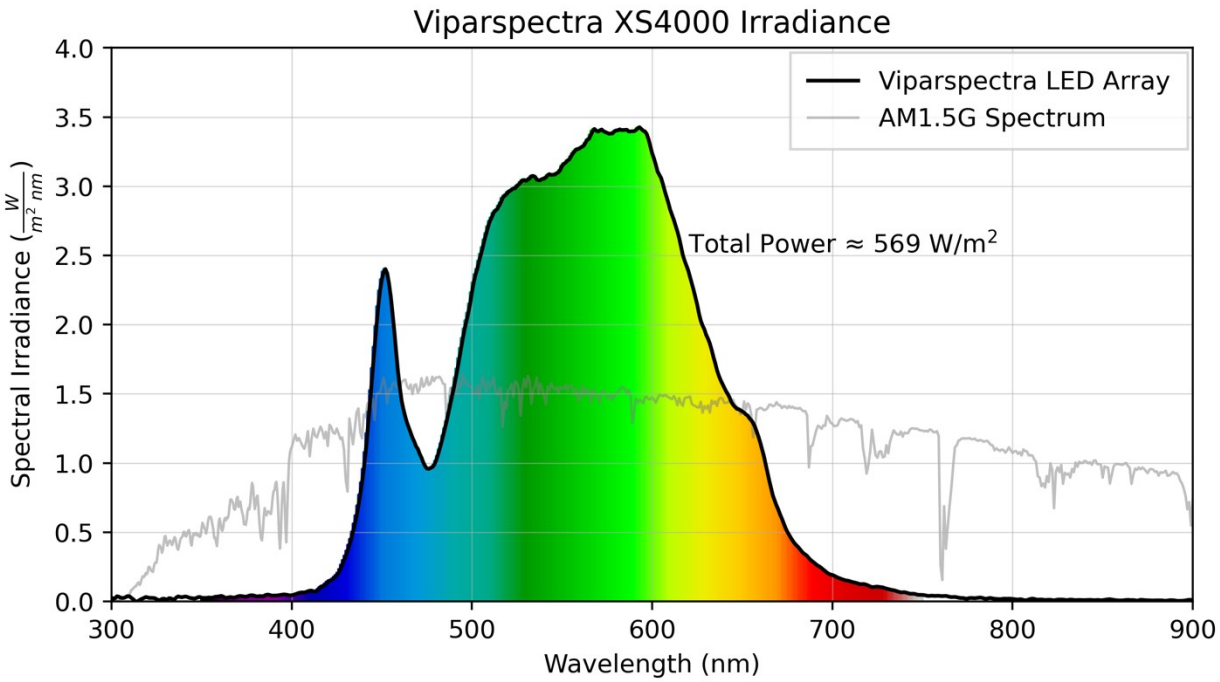

Table S1. R^2 values of linear fits to Williamson-Hall plots presented in **Figure S14**.

R^2		NH_4	MA	EA	iPA	nPA	nBA
Fresh	0.1M	0.89	0.98	0.99	0.98	0.99	0.99
	0.2M	0.72	0.90	0.86	0.99	0.98	0.69
	0.3M	0.77	0.49	0.99	0.99	0.95	0.89
Aged	0.1M	0.69	N/A	0.66	0.84	0.93	0.99
	0.2M	0.43	N/A	0.38	0.85	0.77	0.91
	0.3M	0.50	N/A	0.84	0.99	0.91	0.80